International Journal of Thermal Sciences 66 (2013) 8–18

Contents lists available at SciVerse ScienceDirect

International Journal of Thermal Sciences

journal homepage: www.elsevier.com/locate/ijts

# Local Nusselt number enhancement during gas–liquid Taylor bubble flow in a square mini-channel: An experimental study

Abhik Majumder, Balkrishna Mehta, Sameer Khandekar*

*Department of Mechanical Engineering, Indian Institute of Technology Kanpur, Kanpur 208016, UP, India*

ARTICLE INFO

*Article history:*
Received 3 May 2012
Received in revised form
5 November 2012
Accepted 8 November 2012
Available online 23 December 2012

*Keywords:*
Mini-channels
Taylor bubble flow
Local Nusselt number
Heat transfer enhancement

ABSTRACT

Taylor bubble flow takes place when two immiscible fluids (liquid–liquid or gas–liquid) flow inside a tube of capillary dimensions within specific range of volume flow ratios. In the slug flows where gas and liquid are two different phases, liquid slugs are separated by elongated Taylor bubbles. This singular flow pattern is observed in many engineering mini-/micro-scale devices like pulsating heat pipes, gas–liquid–solid monolithic reactors, micro-two-phase heat exchangers, digital micro-fluidics, micro-scale mass transfer process, fuel cells, etc. The unique and complex flow characteristics require understanding on local, as well as global, spatio-temporal scales. In the present work, the axial streamwise profile of the fluid and wall temperature for air–water (i) isolated single Taylor bubble and, (ii) a train of Taylor bubbles, in a horizontal square channel of size 3.3 mm × 3.3 mm × 350 mm, heated from the bottom (heated length = 175 mm), with the other three sides kept insulated, are reported at different gas volume flow ratios. The primary aim is to study the enhancement of heat transfer due to the Taylor bubble train flow, in comparison with thermally developing single-phase flows. Intrusion of a bubble in the liquid flow drastically changes the local temperature profiles. The axial distribution of time-averaged local Nusselt number ($\overline{Nu}_z$) shows that Taylor bubble train regime increases the transport of heat up to 1.2–1.6 times more as compared with laminar single-phase liquid flow. In addition, for a given liquid flow Reynolds number, the heat transfer enhancement is a function of the geometrical parameters of the unit cell, i.e., the length of adjacent gas bubble and water plug.



## 1. Introduction

Transport mechanisms of heat, momentum and mass under two-phase flow conditions in mini-/micro systems are greatly affected by the local distribution of phases, or flow patterns in the channel. The two-phases may be composed of gas–liquid two-component system or a vapor–liquid single-component system (in the context of the present study, we restrict the discussion to gas–liquid two-component systems; however, it is noted that non-miscible liquid–liquid two-component systems can also give rise to unique transport mechanisms). Slug flow is one of the important multi-phase flow patterns, which belongs to a class of intermittent flows. Taylor bubble train flow, a sub-set of slug flows, is typically characterized by a sequence of long bubbles which are trapped in between liquid slugs. Typically, in mini-/micro-scale systems, when surface tension dominates over gravitational body force, Taylor bubbles adopt the characteristic capsular shape, with a liquid thin film separating the gas/vapor phase with the wall. Such Taylor bubble train flows in confined mini-/micro-scale geometries have singular distinctive local thermo-hydrodynamic transport features. This is due to their intermittent nature, dominance of surface tension, interfacial dynamics, geometrically confined bubbles, effect of local wettability resulting in enhanced heat/mass transport [1].

Under laminar flow conditions, viscous forces interact with surface tension, giving rise to Capillary number scaling ($\mu U/\sigma$). The existence of a thin film surrounding the Taylor bubbles gives rise to bubble slip motion i.e., a higher bubble velocity than the total superficial velocity of the flow defined by $U_b = \psi \cdot J_{tot}$. Film thickness depends on the Capillary number, channel geometry and local wettability between fluids and tube/channel wall (hydrophobic or hydrophilic) [2,3]. For very thin films (sub-microns) around Taylor bubbles, which may form at very low *Ca* and/or flows in super-hydrophobic ducts, interaction of additional disjoining pressure with the flow field has also been argued [1].

Understanding of the species transport under such a flow configuration is quite a challenging problem. In recent years, research on Taylor bubble train flow has increased due to development of mini-/micro-scale systems in diverse branches wherein such flows are encountered such as, ranging from bio-medical, bio-chemical to

* Corresponding author. Tel.: +91 512 259 7038; fax: +91 512 259 7408.
*E-mail address:* samkhan@iitk.ac.in (S. Khandekar).

1290-0729/$ – see front matter © 2012 Elsevier Masson SAS. All rights reserved.
http://dx.doi.org/10.1016/j.ijthermalsci.2012.11.003

**Nomenclature**

| | |
|---|---|
| $A$ | area of cross-section ($m^2$) |
| $C_p$ | specific heat at constant pressure (J/kg K) |
| $D_h$ | hydraulic diameter (m) |
| $\Delta f$ | number of frames (−) |
| $h$ | heat transfer coefficient ($W/m^2$ K) |
| $J$ | superficial velocity (m/s) |
| $k$ | thermal conductivity (W/m K) |
| $\ell$ | length specified in image (m) |
| $L$ | length of the channel, characteristic length (m) |
| $m$ | ratio of relative velocity to bubble velocity (−) |
| $N$ | number of bubble observation (−) |
| $n$ | frames per second ($s^{-1}$) |
| $Q$ | volumetric flow rate ($m^3/s$) |
| $R$ | radius (m) |
| $q''$ | heat flux ($W/m^2$) |
| $t$ | time (s) |
| $T$ | temperature (K) |
| $T^*$ | non-dimensional temperature ($= T - T_{fi}/(q'' \cdot D_h)/k_l$) |
| $U$ | velocity (m/s) |
| $Z$ | distance from inlet (m) |
| $Z^*$ | thermal non-dimensional distance ($=Z/Re \cdot Pr \cdot D_h$) |

*Greek symbols*

| | |
|---|---|
| $\alpha$ | thermal diffusivity ($m^2/s$) |
| $\delta$ | liquid film thickness (m) |
| $\xi$ | volume flow ratio (−) |
| $\varepsilon$ | void fraction (−) |
| $\vartheta$ | frequency of bubbles (Hz) |
| $\mu$ | dynamic viscosity (Pa s) |
| $\rho$ | mass density ($kg/m^3$) |
| $\psi$ | ratio of bubble velocity to total superficial velocity (−) |
| $\sigma$ | surface tension (N/m) |

*Non-dimensional numbers*

| | |
|---|---|
| $Ca$ | Capillary number ($\mu_l \cdot U_b/\sigma_l$) |
| $Nu$ | Nusselt number($h \cdot D_h/k_l$) |
| $Pr$ | Prandtl number ($\mu_l \cdot c_p/k_l$) |
| $Re$ | Reynolds number ($\rho_l \cdot J_l \cdot D_h/\mu_l$) |
| $We$ | Weber number ($\rho_l \cdot U_b^2 \cdot D_h/\sigma_l$) |

*Subscripts*

| | |
|---|---|
| $b$ | bubble, bulk |
| $l$ | fluid |
| $fi$ | fluid inlet |
| $g$ | gas |
| $h$ | hydraulic, hydrodynamic |
| $l$ | liquid |
| $s$ | slug |
| $tot$ | total |
| $uc$ | unit cell |
| $w$ | wall |

thermal management of electronics, water management of fuel cells, micro-two-phase heat/mass exchangers and reactors, nuclear rod bundles, DNA separation and analysis, lab-on-chips, micro-fluidic devices, loop heat pipes, etc. In all the above emerging technologies, Taylor bubble train flow is one of the dominant flow patterns [4–9]. Presence of quasi-periodic slipping bubble interfaces, in front and back of the liquid slugs, modifies the flow field inside the liquid slugs compared with conventional fully developed parabolic profiles as in single-phase flows. Interaction of the ensuing wall shear gradients and free-slip boundary condition at the bubble–liquid interface gives rise to strong circulation inside the liquid slugs [10–12]. These recirculation patterns within the liquid slugs enhance heat and mass transfer from liquid to wall and interfacial mass transfer between gas/vapor and liquid [13–17]. Thus, bulk transport mechanisms are influenced by the dynamics of the local isolated 'unit cell', consisting of a Taylor bubble and adjoining liquid slug. Understanding transport mechanism necessitates localized experimental observations of Taylor bubble train systems, with synchronized measurements of the resulting fluctuations in local conditions such as temperature, pressure and wall heat flux [18]. Mass transfer characteristics are also affected by the local hydrodynamics of the flow (bubble velocity, slip velocity, length of the liquid slug, shape of the bubble–liquid interface) [19]. Knowledge of local thermo-hydrodynamic characteristics of the unit cell during Taylor bubble train flow is vital for complete understanding of the behavior and improving the performance of micro-thermo-fluidic and micro-chemical systems that operate in this regime.

Many mini-/micro fabrication techniques, such as laser machining, chemical etching, micro-milling, abrasive jet machining etc., lead to channels of non-circular cross-section. Rectangular microchannels are of particular interest as they are used extensively in heat sinks of microelectronic devices, as well as for catalytic reactors for micro-fuel processors, biological sensors, lab-on-chip devices, water management of PEM fuel cells, high heat flux dissipating heat exchanger equipment, micro-fluidic devices, etc. While most of the classical works on Taylor bubbles are confined to circular channels and ducts with primarily upward flow configuration. Local transport measurements in rectangular channels are needed to design many upcoming mini-/micro-scale systems. Amongst rectangular channels, a square channel provides the least wetted perimeter, for a given cross-sectional area, and therefore, is preferable from an overall pressure drop point of view. Any other rectangular variant, having the same cross-sectional area as of the square channel, leads to higher wetting perimeter; this decreases the hydraulic diameter, thereby increasing the pressure drop per unit length in the streamwise direction.

In this work, we undertake local heat transfer measurements of air–water Taylor bubble train flow in a square channel of cross-section 3.3 mm × 3.3 mm (aspect ratio ≈ 1). Gas volume flow ratio is the variable parameter. Constant heat flux boundary condition is provided at the channel bottom wall, while the other three sides are kept insulated. To estimate the local and average Nusselt number for a given heat flux condition, local temperature measurement of fluid at the center of the channel cross-section and the wall temperature at corresponding axial location along the streamwise direction, has been done for air–water (a) isolated Taylor bubble and (b) Taylor bubble train flows. Before commencing the two-phase experiments, benchmarking of the setup is done against single-phase data. Additionally, single-phase data has also been compared with trends obtained from three-dimensional numerical simulation of the experiment (hydrodynamically fully developed but thermally developing single-phase flow in one-side heated square channel, under H2 boundary condition, i.e., applied heat flux is constant axially as well as in the transverse direction) on a commercial platform (Ansys-Fluent®V6.3.26).[1] The simulation has also addressed the issue of discrepancy between the bulk-mean

[1] For brevity, details of the CFD simulations are not included here but it can be obtained from Ref. [20].

fluid temperature and the experimentally obtained local center point fluid temperature, for estimating the local Nusselt number. Enhancement of heat transfer due to the Taylor bubble train flow configuration, as compared to thermally developing (but hydrodynamically fully developed) single-phase flow has been scrutinized.

## 2. Literature review

The definitive pioneering work on Taylor bubble flows, for configurations involving conventional circular channels is that of Bretherton [21], who observed that a Taylor bubble does not rise spontaneously in a water filled vertical capillary under the effect of gravity for $Bo < 1.835$. Harmathy [22] and White and Beardmore [23], both contemporaries of Bretherton [21], also addressed this problem. When a gas bubble displaces a wetting fluid which is filled in a capillary, a liquid film is deposited on the capillary wall [24]. This film thickness follows the scaling $(\delta/R) \sim Ca^{1/2}$ for $Ca$ ranging from $10^{-5}$ to $10^{-1}$. Seminal analytical work, with some simplified assumptions by Bretherton [21] established the scaling as $(\delta/R) \sim Ca^{2/3}$, the theory being valid for creeping flows at low $Ca$ ranging from $10^{-3}$ to $10^{-2}$ and bubble Weber number $\ll 1$. Empirical correlation for determining the fraction of the liquid deposited on the tube wall can be casted in terms of the bubble drift velocity, $m$, given by:

$$m = (U_b - U_s)/U_b \tag{1}$$

Thus, as noted earlier, the bubble velocity is somewhat faster than the average liquid slug velocity due to the presence of the liquid film around it. As this drift or relative velocity depends on the film thickness surrounding the bubble, it is obvious that the scaling for film thickness as a function of $Ca$ should, in general, be also applicable for $m$. Indeed, as per Fairbrother and Stubbs [24], $m$ scales as $\sim Ca^{1/2}$ while as per Bretherton [21], it scales as $\sim Ca^{2/3}$. Such scaling typically applies to low $10^{-3} < Ca < 10^{-2}$. When inertia forces become dominant and liquid film thickness gets limited by the thickness of the boundary layer that develops in the liquid as it moves, the parameter $m$ asymptotically approaches a constant value $\sim$0.56–0.60 at large Capillary numbers [25–27]. Taylor [25] also proposed the presence of circulation patterns with paired vortices in the liquid slug for cases where $Ca$ is low (for cases when $m < 0.5$). As $Ca$ increases (for $m > 0.5$), vortices in the liquid slug tend to disappear, leading to bypass flows [26]. More recent experimental and numerical studies [12,28,29] have also confirmed these findings. Some PIV and visualization studies have also been undertaken which confirmed existence of the circulations inside the liquid slug [30].

Kolb and Cerro [31] experimentally studied vertical downward flow of long Taylor bubble flows in a square capillary of size 2 mm × 2 mm. By flow visualization technique, authors proposed a distinct transition (recirculation to complete bypass) of flow field based on $Ca$ ($\geq$0.54). It was also reported that the shape of bubble cross-section is dependent on the flow $Ca$. When $Ca \leq 0.1$, the bubble cross-section is non-axisymmetric but for $Ca > 0.1$, bubble cross-section becomes axisymmetric. As $Ca$ decreases, suggesting an increase of surface tension forces vis-à-vis viscous forces, the pressure field is strongly affected by the local Young–Laplace conditions, on the bubble–liquid interface. The corners manifest a smaller radius of curvature as compared with sections of the tube wall away from the corners and thus, liquid flows more slowly in the corners. Therefore in square channels, the shape of the gas–liquid interface, which is defined by the pressure field, may not be axisymmetric for low $Ca$.

Thulasidas et al. [11,12] developed a mass balance model for Taylor bubble train flow to compute different transport parameters, such as the size and shape of bubbles, bubble velocity and volume flow ratio through capillaries of different shapes and sizes. The non-dimensional velocity, $U_b/J$ was also experimentally determined in circular and square capillaries. Results were in good agreement at higher $Ca$ for both kinds of capillaries; however, at small $Ca$, the discrepancy in $U_b/J$ was larger for square capillaries, unlike the circular one. Kamisli [32] numerically studied flow of long bubble in a square capillary and suggested that the liquid deposited on capillary wall is a function of flow $Ca$. Pressure drop and wetting film thickness for isolated bubble and bubble trains moving in circular and square capillaries, at different Capillary number, has been studied in [33,34]. The discrepancies observed amongst the available analytical correlations, experimental data and computational results, for predicting the film thickness in square capillaries at low $Ca$, were reported. Van Baten et al. [35,36] numerically studied hydrodynamics of slug flow in capillaries and computed the bubble slip velocity. Ide and Matsumura [37], Mishima et al. [38], Wambsganss et al. [39], and more recently, Chen et al. [40] have investigated flow pattern transition and frictional pressure drop in different rectangular channels having a wide range of aspect ratios and reported correlations to predict the frictional pressure drop and the Chisholm's factor. Han and Shikazono [41] measured the liquid film thickness in micro-square capillaries of different sizes and for different fluids, using laser focus displacement meter. In this study, it was also reestablished that at low $Ca$ ($\leq$0.1) bubble cross-section is generally non-axisymmetric. Wörner [42] has presented a comprehensive review on Taylor flow in narrow circular and rectangular channels. In this study, all major correlations which relate the parameter $m$ with the flow $Ca$ have been scrutinized. It was concluded that ratio of bubble velocity $U_b$ to the total superficial velocity $J_{tot}$ is a key parameter to characterize Taylor slug flows.

Bao et al. [43] experimentally investigated non-phase-change air–water Taylor flow in a circular channel of diameter 1.95 mm under constant heat flux boundary condition and observed enhancement in heat transfer coefficient due to the presence of gas bubbles. Narayanan and Lakehal [44] conducted numerical simulation of sensible heat transfer during gas–liquid flow in small-diameter pipes and found significant increase in the overall heat transfer due to presence of circulations inside the liquid slugs as compared to single-phase flow. Gupta et al. [45] studied the flow and heat transfer phenomena for a specified flow $Re$ (=280), $Ca$ (=0.006) and homogeneous void fraction (=0.51). In this study, the average Nusselt number showed approximately 2.5 times enhancement as compared to the single-phase liquid flow. Walsh et al. [46] experimentally investigated the heat transfer rate in non-boiling two-phase slug flow in a circular channel of 1.5 mm internal diameter under constant heat flux boundary conditions. InfraRed thermography was employed to measure wall temperature. It was concluded that such a flow pattern can be very useful in augmentation of $Nu$ under fully developed flow; whereas the performance degrades in case of entrance region flow. However, these observations were made without measuring local fluid temperature; estimation of the fluid temperature was done by linear interpolation. Asadolahi et al. [47] numerically studied slug flow by using two different approaches: (a) fixed domain approach (b) moving domain approach, to control length of bubbles and slugs. It was found that in fixed domain approach, obtaining fully developed flow, even in long channel with large number of bubbles, was difficult and computationally expensive. However, in contrast, moving domain approach with periodic boundary condition, fully developed condition could be obtained and controlled length of bubbles and liquid slugs facilitates to observe the effect of lengths on the hydrodynamics and heat transfer. Mehdizadeh et al. [48] numerically studied heat transfer in Taylor bubble flow using Volume-of-Fluid (VOF) method and successfully captured the thin film around the bubbles. Overall enhancement in the heat transfer, up to 610% compared to Poiseuille flow was also reported in this

study. Asadolahi et al. [49] simulated a 'unit cell' with periodic boundary condition and frame of reference moving with the bubble in 2 mm circular capillary for $22 \leq Re_{TP} \leq 1189$ and $0.003 \leq Ca \leq 0.16$. It was found that for $Re_{TP} \geq 951$, axisymmetric assumption of circular geometry did not hold. Leung et al. [50] experimentally studied the effect of gravity on Taylor bubbles in horizontal mini-channels of internal diameters 1.12 mm, 1.69 mm and 2.12 mm, using micro-PIV. Parabolic drainage velocity profile was obtained and it was concluded that heat transfer was not affected by gravity. Zaloha et al. [51] also used micro-PIV to study the hydrodynamics of the gas–liquid Taylor flow in non-circular straight and meandering microchannels. Study concluded that recirculations exist inside the liquid slugs and recirculation velocity linearly varies with total superficial velocity. Talimi et al. [52] numerically investigated the slug flow using moving frame of reference and concluded that this approach of simulation over-predicts the pressure drop and heat transfer, as compared to fixed domain approach. It was also observed that Taylor flow in which thin film was absent around the gas phase, heat transport was higher. Talimi et al. [53]have presented an extensive review on the numerical studies of Taylor slug flow. This review indicated that hydrodynamics and heat transfer of Taylor slug flow in the non-circular ducts requires much more explorations with different thermal boundary conditions.

This extensive review of literature suggests that work done on heat transfer in Taylor bubble train flow is primarily confined to circular channels with conventional thermal boundary conditions, viz., uniform heat flux or uniform wall temperature. In addition, not many local heat transfer experimental data are available in the open literature; mostly, the problem has been tackled through computational simulations. Many modern mini-/micro-channel based systems are, in general of non-circular cross-sections and mostly employ non-standard thermo-hydrodynamic boundary conditions, either by design or by specific constraints due to manufacturing routes. Therefore, investigation of heat transfer in Taylor bubble train flow and local transport measurements in non-circular mini-/microchannels is needed to design many upcoming engineering systems.

## 3. Experimental details, procedure and data reduction

The experimental setup is designed to investigate thermo-hydrodynamics of air–water (a) Isolated Taylor bubble flow and (b) Taylor Bubble Train flow, in a horizontal square capillary of 3.3 mm × 3.3 mm cross-section. Schematic of the experimental setup is shown in Fig. 1(a) and (b) and dimensional details of the heater, including exact positioning of wall thermocouples, is shown in Fig. 1(c). A constant heat flux boundary condition was applied at the bottom wall of the channel (by a DC-strip heater), while other three sides of the channel were kept insulated. Heat loss to the surroundings was calculated and it was not more than 17% of the heat input in any of the experiments. The side walls of the channel were made of borosilicate glass ($k$ = 0.744 W/m-K and thermal diffusivity $\alpha = 4.44 \times 10^{-7}$ m$^2$/s) for insulation as well as visualization of the Taylor bubble flow by using Photron-Fastcam®-SA3 high-speed camera. Image acquisition was done at 1000 fps for all the Taylor bubble train flow experiments. A single syringe infusion pump (model Cole-parmer-WW-74900) was used to inject air with precisely controlled flow rate at the T-junction, as shown in Fig. 1(b). The T-junction was located sufficiently upstream of the heated test section for achieving stability of flow inside the heated test section. Micro-thermocouples (Type-K, 0.13 mm bead diameter, Omega®) were used to measure the local wall and fluid temperatures at three measurement stations. The time constant of these thermocouples was of the order of $10^{-4}$ s, which ensured reliable dynamic response. Thermocouples measuring the local fluid temperatures were inserted from the top of the channel and were centrally located in its cross-section, as shown in Fig. 1(a). Thus, these three thermocouples measured the liquid temperature at the center of the channel cross-section, not the bulk-mean temperature of the fluid. Here, the fact that true bulk-mean temperature cannot be estimated by intrusive thermometry should be appreciated; the implications of this discrepancy have been addressed by computational simulation, as will be detailed in Section 4.1. In spite of this apparent discrepancy, these three thermocouples do provide valuable local information, especially for the Taylor bubble train flow situation. Interfacial distortion of Taylor bubbles interfaces during the flow, due to these thermocouples, was not observed. However, these thermocouples did disturb the liquid flow, as will be discussed later. Three thermocouples at the wall were located at a distance of 0.5 mm from the actual fluid–solid interface, as shown in Fig. 1(c). Due to the construction of the heater assembly, there was an offset of 0.6 mm in the location of theses thermocouples from the central axis, as detailed in Fig. 1(a) and (c). A 24-bit PC data acquisition system (National Instruments® NI-9213) was used with LabView®PC interfacing. Data acquisition has been done at 20 Hz, which satisfies the Nyquist criterion. Constant inlet fluid (distilled, deionized and degassed water) temperature was maintained within ±0.01 °C by a circulator (Julabo® ME-26). The air and water flows were respectively controlled with the help of flow control valves. The experiment was conducted in two steps. At first, data was recorded for steady-state single-phase (water) flow at a defined flow rate. Then, in the next step, keeping the liquid flow rate identical, air was injected through the T-junction at a controlled rate to create either, (i) a single isolated bubble flow or, alternately (ii) a quasi-periodic Taylor bubble train flow; simultaneously, thermocouple data and image acquisition was undertaken for subsequent data reduction, as explained next.

### 3.1. Data reduction

The values of fluid and wall temperature are non-dimensionalized as follows:

$$T^* = \frac{T - T_{fi}}{(q'' \cdot D_h)/k_l} \tag{2}$$

where, $T = T_f$ or $T_w$, as per the case; $q''$ and $T_{fi}$ being specified for a given run.

The local, time-averaged Nusselt number along the flow direction is defined as:

$$\overline{Nu}_z = \frac{q'' \cdot D_h}{\left(\overline{T_w} - \overline{T_b}\right) \cdot k_l} \tag{3}$$

As noted, the three thermocouples inserted in the fluid flow domain measure the local fluid temperature and not the bulk-mean fluid temperature. Therefore,

For experimental data reduction:

$\overline{T_w}$ = local wall temperature of the point where thermocouples are embedded

$\overline{T_b}$ = local fluid temperature measured at center of the cross-section along the channel axis

For each experimental run, $\overline{T_w}$ and $\overline{T_b}$, respectively, are estimated from the local thermocouple data integrated over 60 s (at 20 Hz we get 1200 data points), after achieving quasi-steady state flow conditions. The experimentally obtained fluid temperature $\overline{T_b}$ is not equal to the actual bulk-mean temperature of the fluid. As intrusive measurements cannot provide the true value of the bulk-mean temperature, the possible ways of estimating this value are

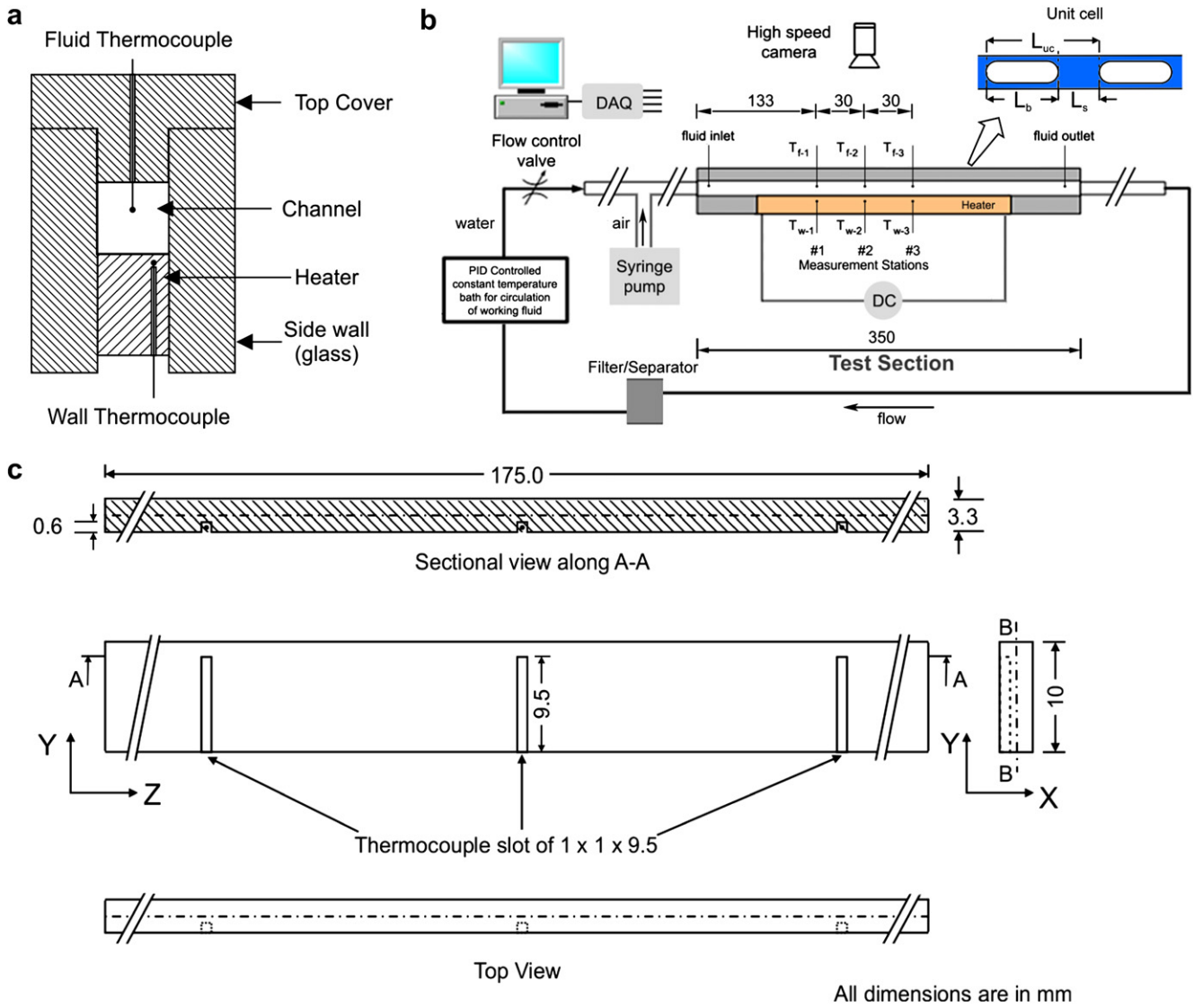


**Fig. 1.** (a) Details of the test section, (b) schematic details of the experimental test rig, and (c) dimensional details of the heater.

(a) suitable interpolation by using the average inlet and outlet temperatures, which is routinely done, especially for constant heat flux boundary conditions without any conjugate effects. Such interpolated values of the bulk-mean temperature are then used to estimate the Nusselt number or, (b) numerically simulating the entire flow condition; this provides the exact bulk-mean temperature and therefore the true Nusselt number, provided of course, the simulation is comprehensively validated. Therefore,

For numerical data reduction:

$\overline{T_w}$ = peripheral averaged wall temperature at axial location of interest along the channel

$\overline{T_b}$ = area averaged bulk-mean fluid temperature at the fluid cross-section of interest along the channel, as obtained computationally.

By adopting the above mentioned data reduction scheme, the local Nusselt number obtained from Eq. (3) will naturally be different when estimated from experimental data and numerically obtained data. For a heated channel, experimentally obtained $\overline{T_b}$, which represents the local fluid temperature measured along the central axis of the channel cross-section, will be smaller than the corresponding true bulk-mean temperature obtained by computational simulation, leading to a lower conservative estimation of the true local Nusselt number. While this is true for single-phase flow, in the Taylor bubble train flow case, toroidal vortices exists in the liquid slug which enhances mixing of the fluid, i.e. the temperature profile in the liquid slug will be comparatively more uniform, or, the variation in the fluid temperature across channel cross-section at any given streamwise location will be comparatively smaller. This will result in a much smaller discrepancy in the estimated local Nusselt number for the Taylor bubble train flow, as compared with its true value, based on the correct bulk-mean temperature.

Mean bubble velocities are calculated from digital analysis of images obtained from high-speed photography. In the acquired images, a rectangular observation window of known dimension is fixed in the flow domain, and the number of frames required for a bubble to pass through this reference window is calculated. As the high-speed image acquisition rate is known, bubble velocity can thus be ascertained. If $N$ is the number of bubbles tracked for estimating the average bubble velocity $U_b$, $n$ represents the fame rate of image

capture, ℓ represents the length of the observation window and $\Delta f$ is the number of frames required for a bubble to pass through the window, then:

$$U_b = \frac{1}{N}\sum_{i=1}^{N}\left(\frac{\ell}{\Delta f}\right)_i n \tag{4}$$

For the present range of experiments, values chosen for the estimation of average bubble velocity $U_b$ are, $N = 25$, $n = 1000$ frames/s and $\ell = 25$ mm. The sequence of images also provides us the average time required for the unit cell to pass through a fixed observation point, $t_{uc}$. This provides the necessary bubble frequency, given by:

$$\vartheta = 1/t_{uc} \tag{5}$$

In the analysis of gas–liquid Taylor bubble train flow, it is noted that the ratio of liquid to gas-phase density and viscosity, respectively, is very high. The flow is incompressible and when a train of 'unit cells' is flowing through a channel, it is assumed that respective lengths of the bubbles and liquid slugs will practically remain constant. Though, this assumption is not completely satisfied all the time during experiments, yet careful and controlled execution of experiments can keep the variation of bubble and slug lengths within reasonable limits. Success depends on precise maintenance of the flow rates of gas and liquid phases, and design of the T-junction for generating Taylor bubbles. In the present experimental measurements, variations in the bubble/liquid slug lengths and velocities are not more than ±7%. This has been estimated from the image analysis of large number of bubbles and slugs (typically, 25 unit cells). Based on this assumption, the Taylor bubble flow hydrodynamics is completely described by making the length of a unit cell ($L_{uc} = L_b + L_s$) as the basis. Basic definitions describing the Taylor slug flow are summarized in Appendix (Eqs. (A1)–(A9)). Based on these definitions, $L_s$, $L_b$, $U_b$, $U_s$, $Ca$, $\psi$, $\xi$ and $\varepsilon$ are calculated. Calculation of $U_b$ is done by the analysis of images captured at high speed. Average liquid slug velocity $U_s(=J_{tot})$ is determined by using global mass balance, Eqs. (A5) and (A6), or by Eq. (A7) for the liquid phase, in a frame of reference moving with the bubble [42].

Some basic hydrodynamic flow characteristics for the present experiments are presented here. In Fig. 2, average void fraction $\varepsilon$, calculated by using Eq. (A3), is plotted against the volume flow ratio $\xi$ and validated with data available in the literature [54,55]. The data by Hayashi et al. [54] was generated on circular tubes and therefore the ratio of $\varepsilon/\xi$ will be higher for this case than square channels, as observed. The Armand correlation [55] also corresponds to flow in circular channels. It is observed that the present experimental data trends are in good quantitative agreement. In Fig. 3, $U_b/J_{tot}$ is plotted as function of $Ca$ and compared with some available benchmark experimental results. As the $Ca$ of the present experimental investigation is very low, so the scatter in the data is quite high as can be seen in the figure; such a scatter is also reported by Thulasidas [11]. Over the years, several authors have pointed out the discrepancy in experimental data scaling at low Capillary numbers. Ironically, classical theories, even the seminal theory of Bretherton [21], which was based on creeping flows at low $Ca$ ranging from $10^{-3}$ to $10^{-2}$ and bubble Weber number $\ll 1$, could not predict the discrepancy in film thickness and therefore the ensuing slip. This discrepancy has been explained by various mechanistic models and arguments [32,33], the most convincing being the effect of variable surface tension in the film and the bubble cap region, which in turn increases the film thickness at low $Ca$ [34]. Other arguments point toward local variations of the interphase slip due to drainage inconsistencies and fluctuations in the film thickness at low $Ca$ [31].

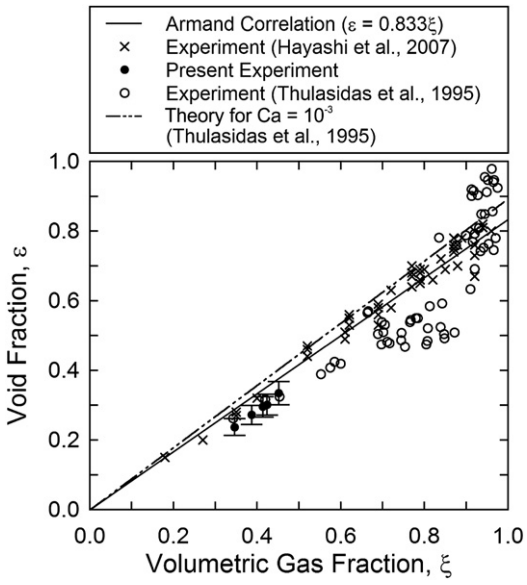


**Fig. 2.** Variation of void fraction with volumetric gas fraction.

## 4. Results and discussion

### 4.1. Benchmarking with single-phase experiments and numerical simulation

Benchmarking of the experimental setup has been first done by conducting single-phase liquid flow experiments. Several tests have been conducted to obtain axial variation of non-dimensional wall and fluid temperatures for single-phase flow in one-side heated square channel with constant heat flux. In all the experiments, flow conditions are hydrodynamically developed but thermally developing. Actual thermal development length inside the heated test section length (175 mm) is a function of flow $Re$, for a given inlet $Pr$. A long channel constructed prior to the heated test section ensured full hydrodynamic flow development for the entire range of experimental flow $Re$. For hydrodynamically fully developed but thermally developing flow in a square channel with four-side heating, Shah and London [56] have suggested thermal entry length of $Z_{th} = 0.066 \cdot Re \cdot Pr \cdot D_h$. If the channel would have been heated by four sides it follows that, for $Re \leq 40$, all three

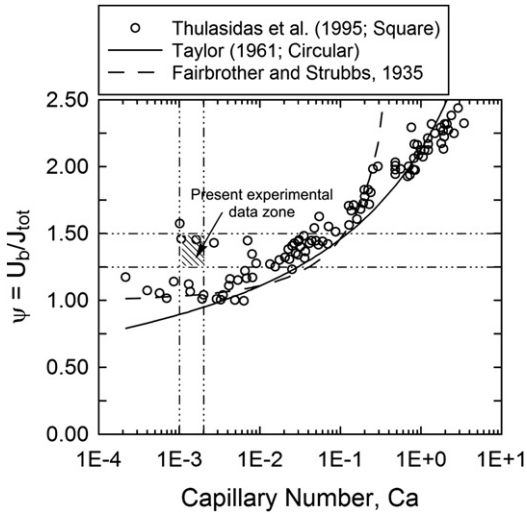


**Fig. 3.** Variation of bubble velocity ratio with the Capillary number.

thermocouple measurement stations would be lying in the hydrodynamic as well as thermally fully developed regions, whereas, for $Re \geq 115$ all of them would fall in hydrodynamically developed but thermally developing regions. For one-side heated square channel, i.e., the present case, thermal development length will always be more than the four-side heated channel. Thus, for the present range of *Re*, flow is indeed in thermally developing region only; all the present cases are therefore of Graetz type.

In Fig. 4(a) experimental temperature profiles of single-phase water flow for $Re = 120$, 180 and 220 respectively, are shown and are also compared with the results obtained by numerical simulation of the exact experimental conditions. From the experimental results, the developing nature of flow is quite clear. Secondly, as the flow *Re* increases, length of the test cell is quite insufficient for thermal development of the flow. At low flow rate ($Re = 120$), the degree of thermal development increases within the test section length, as compared with that at flow $Re = 220$. There is a small difference between the wall temperatures obtained from the simulation, as compared to experimental values. This difference is due to (i) the wall thermocouple is indeed located, as noted earlier, at a physical distance of about 0.5 mm from the actual fluid-solid interface, as detailed in Fig. 1(a) and (c), (ii) it was not possible to locate the thermocouple exactly at the center plane *B*–*B* of the heater and, (iii) some parasitic heat losses will always remain unaccounted. With these uncertainties, match with the simulation is quite satisfactory.

Fig. 4(b) shows simulated isotherms of the fluid temperature on channel cross-section at three different streamwise locations ($z^* = 0.0131$, 0.0225, 0.0319) at $Re = 220$. The location of the thermocouple bead measuring the temperature during the experiments is indicated by point C on these figures. The table alongside compares simulated bulk-mean temperature, simulated center point temperature (point C) and actual thermocouple measurements. Firstly, simulated values of temperature at point C are nearly identical to the measured values of fluid temperature at those locations, respectively, within the experimental error band. Secondly, the fact that thermocouple is not indicative of the true bulk-mean temperature is quite obvious. These thermocouples measure lower values than the actual bulk-mean temperature.

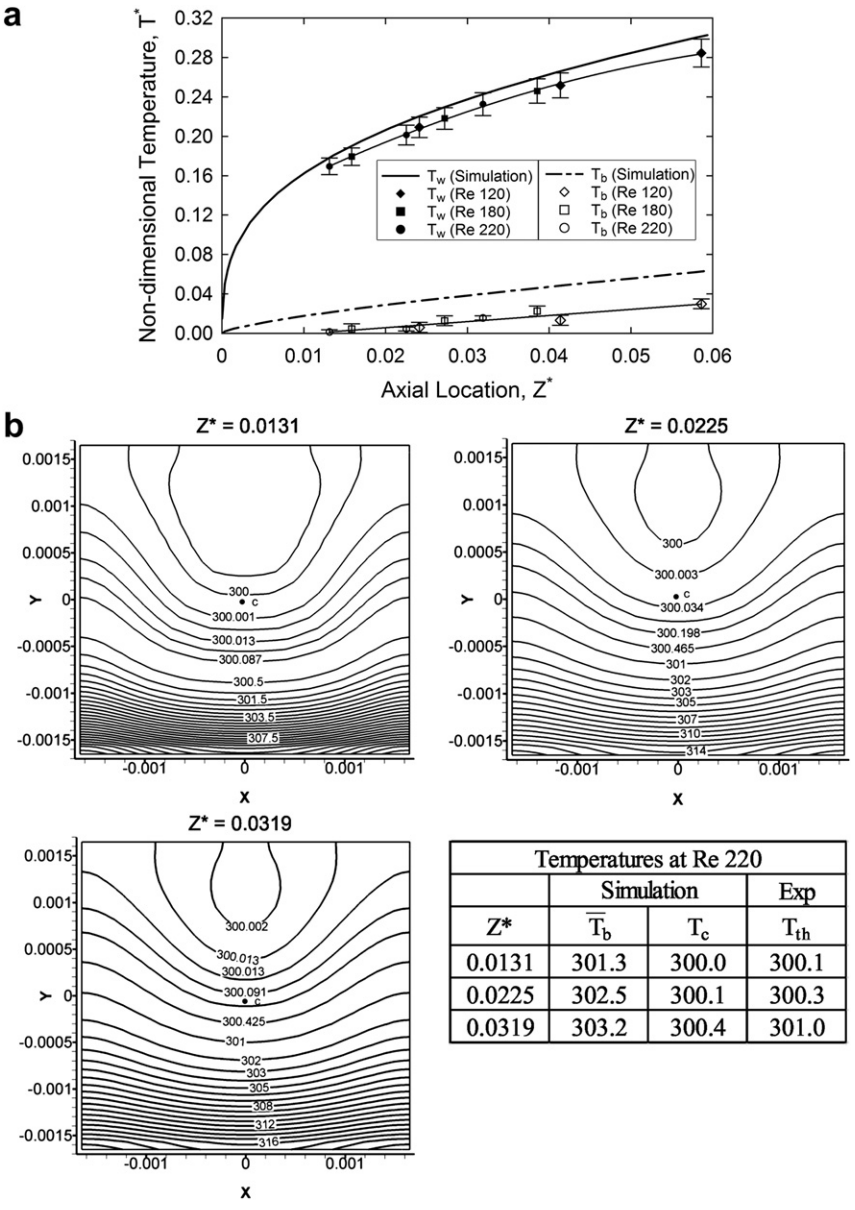


| Temperatures at Re 220 | | | |
|---|---|---|---|
| | Simulation | | Exp |
| Z* | $\overline{T}_b$ | $T_c$ | $T_{th}$ |
| 0.0131 | 301.3 | 300.0 | 300.1 |
| 0.0225 | 302.5 | 300.1 | 300.3 |
| 0.0319 | 303.2 | 300.4 | 301.0 |

**Fig. 4.** (a) Axial variations of non-dimensional wall and bulk fluid temperature and (b) temperature contours for flow *Re* 220.

Thus, Nusselt number calculated from Eq. (3) will be somewhat lower for the thermocouple based estimation than simulation based estimation. The Nusselt number obtained from single-phase simulation and experiments will be compared later in Fig. 8.

### 4.2. Single (isolated) Taylor bubble flow

When steady state is reached in single-phase liquid flow at a given flow rate, a single isolated Taylor bubble is injected in the flow at the T-junction, which is located far upstream in the tube from the heated test section. This ensures that, any flow perturbations created by sudden injection of the bubble gets dissipated by the time this bubble reaches the heated test section. Typical wall and fluid temperature profiles, at the three measurement stations at $Re = 120$ and heat input of 8.0 W, are shown in Fig. 5(a)–(c), for three different isolated bubble lengths, respectively. In the present experiments, wall temperature does not show any appreciable change as the isolated bubble passes through the three measurement stations. This is primarily because of thermal inertia of the heater wall, its response time being slower than the disturbance time scale created by the bubble. However, at any axial location, the air-bubble temperature is seen to be higher than the immediate surrounding liquid, as indicated by the thermocouples located at the three measurement stations inside the fluid domain. This is attributed to the low thermal capacity of air as compared with water. As the applied heat flux is constant along the streamwise direction, the rise in temperature of the air bubble will be higher than the surrounding liquid. Thus, there is an apparent momentary increase of the local heat transfer coefficient, attributed to the decrease in the difference between the wall and fluid temperature. After the isolated air-bubble passes and single-phase water flow is restored, the water temperature comes back to its original level. Flow visualization clearly reveals that the bubbles smoothly pass through the micro-thermocouple without any generation of secondary bubbles or any visual/noticeable interfacial disturbance due to the presence of the micro-thermocouple.

### 4.3. Taylor bubble train flow

Graetz-solution of single-phase fully developed flow suggests an asymptotic constant value of Nusselt number under the applied boundary conditions [56]; hence, limiting the heat transfer coefficient. Enhancement in the thermal transport under such flow conditions can only be achieved by creating local flow disturbances. In the present case, such disturbances have been achieved by the injection of a quasi-periodic continuous Taylor bubble train into liquid flow. This provides the opportunity to study its effectiveness in enhancing heat transfer. As noted earlier, Taylor bubble train flow is achieved by continuous injection of air from a regulated syringe infusion pump, supplying air to the T-junction located far upstream, as shown in Fig. 1(b). The flow rate of the air, and therefore its volume flow ratio is controlled. Results reported here are from experiments carried out at different $\xi$, by changing the injected air flow rate, keeping liquid flow rate constant.

Fig. 6(a)–(c) show the temporal variation of the fluid temperature, wall temperature, their difference and the resulting local Nusselt number at the measurement station 1, 2 and 3 for volume flow ratio $\xi = 0.389$, respectively. As can be seen, injection of Taylor bubble reduces the wall temperature at all measurement stations, as compared to the case when only single-phase liquid was flowing. Simultaneously, an increase in the fluid temperature is also noted, the phenomenon being similar to the single Taylor bubble case (as explained in Section 4.2). Due to intermittent nature of the flow and difference of the thermal capacities of air and water, the fluid temperature fluctuates quasi-periodically with a dominant

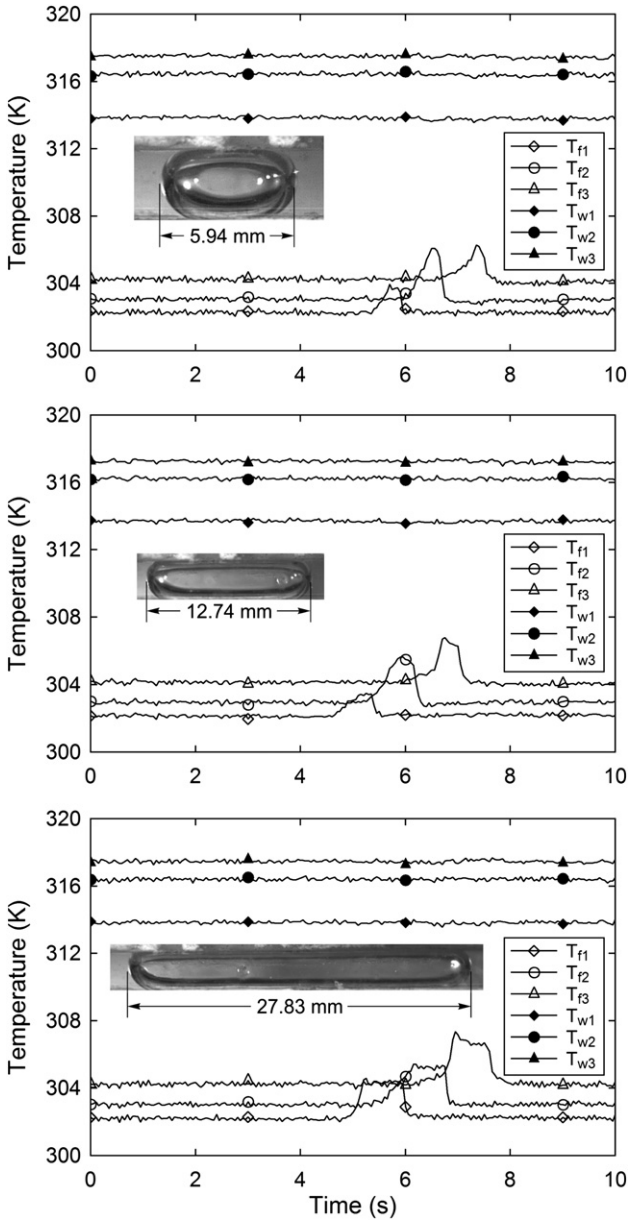


**Fig. 5.** Variation of wall and fluid temperature with time for a single Taylor bubble flow at $Re_l = 130$ of length 5.94, 12.74 and 27.83 mm.

frequency which matches with the bubble flow time scale, as will be discussed in Fig. 7 (see inset in Fig. 6(b)). Wall temperatures continuously decrease after the air injection starts and eventually attain a quasi-steady state. This is due to the enhanced localized radial mixing caused by the local circulation in the liquid slugs trapped between the Taylor bubbles [29]. Typically, for such flow conditions toroidal vortices are present in the flowing liquid slugs which enhance the heat transfer coefficient [29,44,46]. The alternating pattern of liquid slug and bubble flow continually disrupts the formation of thermal boundary layer, which gets renewed every time an air-bubble passes. As can be seen in the figures, wall and fluid temperatures come back to the original level once air injection is stopped and flow returns back to single-phase water flow. Fig. 6(c) clearly indicates that air injection induces strong enhancement in local Nusselt number, which settles down to a new asymptotic high level, once quasi-steady state is attained during air-injection phase. Stopping the air flow brings the Nusselt number back to the level corresponding to the single-phase water flow.

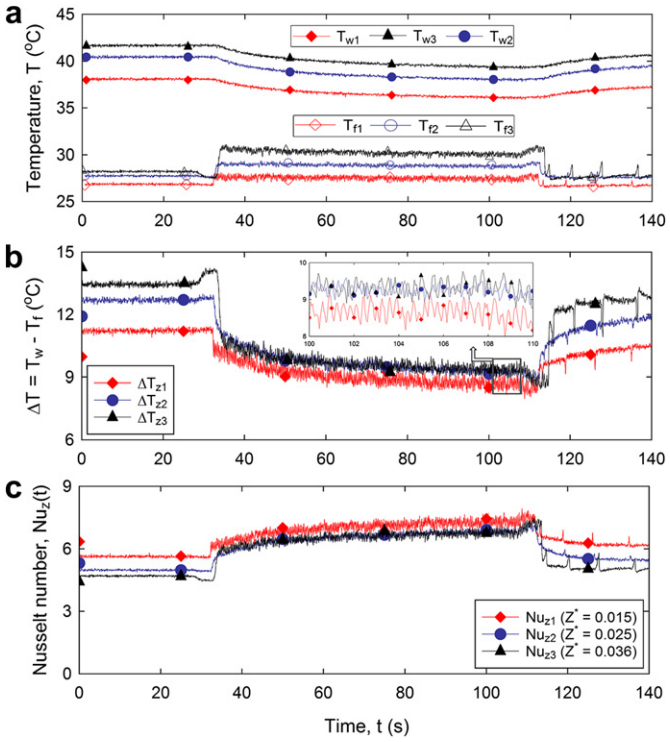


**Fig. 6.** (a) Transient temperature distribution of fluid and wall, (b) transient wall and bulk fluid temperature difference, (c) local Nusselt number variation at measurement station 1, 2 and 3 for volume flow ratio of 0.389 (liquid flow *Re* 196 and heat input 8.0 W).

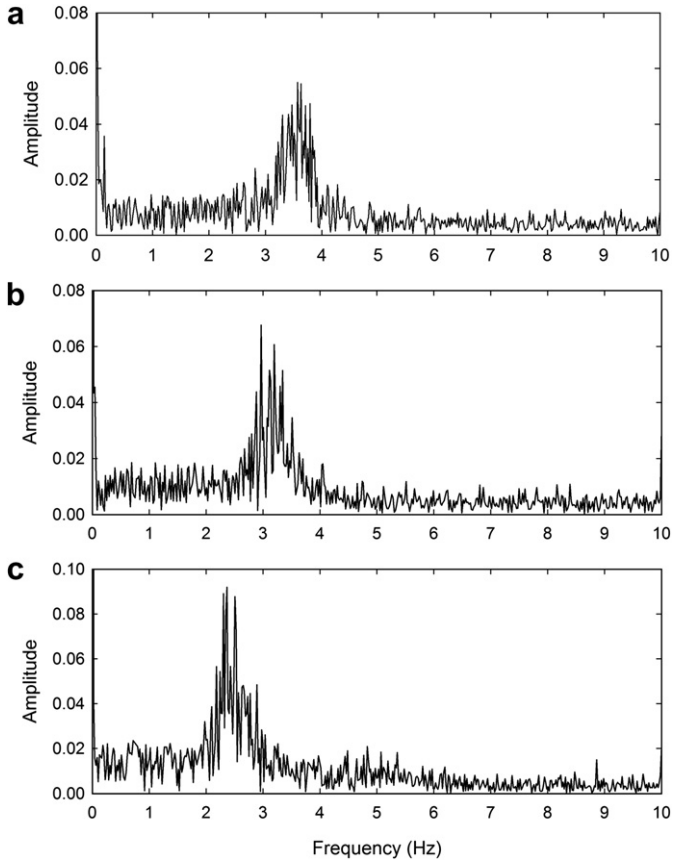


**Fig. 7.** Bubble frequency analysis of temperature data for different volume flow ratios (a) $\xi = 0.45$, (b) $\xi = 0.40$, (c) $\xi = 0.35$ (liquid flow *Re* 196 and heat input 8.0 W).

Fig. 7 shows the power spectrum in frequency domain for the time–temperature data obtained from thermocouple located at measurement station #1 (refer Fig. 6(a)). As indicated earlier, temperature data is acquired at 20 Hz in all the experiments. The dominant frequency is indicated for three different volume flow ratio ($\xi$) at fixed liquid flow $Re = 196$ and heat input of 8.0 W. As can be seen, there is some scatter in the thermocouple data and distinctive narrow spectrum peaks are not obtained. There are two main reasons for this frequency scatter, (a) length of the individual liquid slugs and air bubbles obtained by the injection of air at the T-junction is not completely uniform. This directly affected the temporal thermocouple data, and, (b) invasive nature of the thermocouples during the flow also contributes to the data scatter. The Taylor bubble train flow has also been photographed at 1000 fps to determine the bubble frequency by image analysis. The average bubble frequencies, for volume flow ratios 0.424, 0.389 and 0.321 are 3.60 Hz, 3.25 Hz and 2.43 Hz, respectively, with maximum standard deviation of 8%. As can be seen, power density peaks obtained by the thermocouple data satisfactorily matches with the bubble frequencies obtained through the image analysis, within the inherent range of fluctuations, as delineated above.

For the present range of experiments, axial variation of the time-averaged Nusselt number, computed at three measurement stations is shown in Fig. 8, for single-phase water flow and Taylor bubble train flow experiments. The figure also shows variation of single-phase Nusselt number obtained from simulation, under the boundary conditions as explained earlier (refer Fig. 4). Looking at the experimental results it is noticed that single-phase heat transfer (based on fluid thermocouple temperatures, Fig. 4(a)) is lower, and therefore conservative than its corresponding values obtained by simulation (based on bulk-mean temperature). For the sake of comparison, Nusselt number obtained by simulation, but based on local center point temperature, is also shown. As can be seen, experimental single-phase measurements are quite satisfactory and illustrate the developing nature of flow, Nusselt number gradually decreasing in the streamwise direction, as thermal boundary layer develops. This provided the necessary confidence for conducting the two-phase flow experiments.

Results obtained for the Taylor bubble train flow clearly show that there is a significant enhancement in heat transfer, as compared to single-phase water flow. Streamwise locations in Fig. 8 for the Taylor bubble train flow are normalized by *Re*, based upon total superficial velocity of the two-phase flow. It is also evident that within the present range of experiments, decreases in volume flow ratios decreases $\overline{Nu}_z$; however, an overall enhancement in the heat transfer, as compared with single-phase flow, is still observed at all the measurement locations. Percentage enhancement with respect to the single-phase flow is not high in the early part of the channel. In this part of the thermal entry length, the developing nature of single-phase flow itself provides sufficiently high transport coefficient but, in the latter part of the channel ($Z^* > 0.01$), advantage of Taylor bubble train flow is clearly visible. For benchmarking, different correlations developed for heat transfer in Taylor bubble train flow in circular channel with uniform heat flux condition, are also shown [46,57]. It is observed that Nusselt number data obtained in the present experiments is approximately 1.1–1.3 times lower than the values predicted by the correlations. This is attributed to the difference in thermal boundary conditions for the two cases. It is worthwhile to note that even for fully developed single-phase flow in square channels, a one-side uniformly heated channel provides a Nusselt number which is approximately 1.3 times lower than a channel which is uniformly heated from all four sides [56].

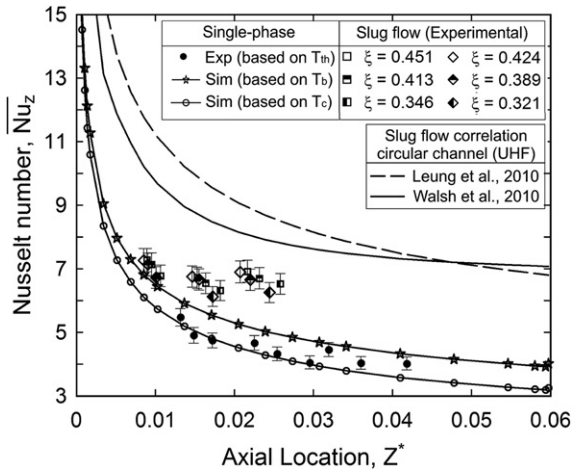


**Fig. 8.** Axial variation of time-averaged local Nusselt at various volume flow ratios.

Another qualitative trend of the thermal transport behavior of Taylor bubble train flow, as against thermally developing single-phase flow is that the Nusselt numbers obtained at all the three measurement stations are rather uniform. Unlike single-phase developing flows, injection of air bubbles disturbs the species boundary layers and the resulting recirculation dynamics quickly sets in a near uniform Nusselt number scenario along the streamwise direction. Decreasing volume flow ratio $\xi$ brings the thermal transport situation asymptotically closer to single-phase liquid flow. In contrast, as $\xi$ increases, the liquid slug length trapped between the Taylor bubbles goes down. This decreases the time scale of the recirculating toroidal vortices, improvising the Nusselt number. Logically, such an enhancement of Nusselt number with $\xi$ will not be monotonous as after a threshold value of $\xi$, the flow morphology may change to churn/annular flow.

## 5. Summary and conclusions

Many engineering applications in mini-/micro-scale require enhanced heat transfer characteristics from convective fluids. Under such geometrical constraints, the ensuing flows are typically laminar with limited heat transport capability. Introduction of simple non-boiling Taylor bubbles in the flow can be an effective strategy for enhancement of local heat transfer, as reported in the present study. The major conclusions of the study are as follows:

- Injection of Taylor bubbles provides an efficient means of heat transfer enhancement, up to 1.2–1.6 times, as compared to fully developed laminar single-phase liquid flow. The relative enhancement may not be very attractive when compared to single-phase flows in the early part of their flow development.
- At any given location in the streamwise direction, flow of Taylor bubble train results in lowering of the wall temperature and increase of the time-averaged fluid temperature. During the Taylor bubble train flow, while temporal fluctuations in the fluid temperature were clearly observable by the embedded micro-thermocouples, local temporal fluctuations of the wall temperature were not detectable in the present study. This was due to the high thermal inertia of the wall as compared to the ensuing time scales of the involved thermo-fluid transport process.
- With the high resolution temporal measurements of local fluid temperature, dominant frequency of the bubble train (unit cell) has been obtained, which compares quantitatively well with values obtained independently from photographic data. There is some scatter in the frequency spectrum, attributed mainly to the inherent perturbations in the bubble lengths obtained by the T-junction air–water injection arrangement.
- Increasing volume flow ratio ($\xi$), for a fixed liquid mass flow rate, the T-junction flow mixing system resulted in longer air bubbles, i.e. smaller liquid slugs entrapped between the bubbles. This increased the time-averaged local *Nu*, for the present range of Taylor bubble train flow experiments. However, such an increase may not be monotonous as increasing volume flow ratio will eventually change the flow pattern; this aspect needs further exploration.

## Acknowledgments

Financial grants from the Indo-French Center for Promotion of Advanced Research (IFCPAR) are gratefully acknowledged. The first author would also like to thank the Quality Improvement Program (QIP) of IIT Kanpur, in association with National Institute of Technology, Agartala, India for supporting his graduate studies at IIT Kanpur, India.

## Appendix

The primary definitions used during the data reduction of the Taylor bubble flow are as follows:

$$\text{Superficial velocities } J_g = \frac{Q_g}{A};\quad J_l = \frac{Q_l}{A};\quad J_{tot} = J_g + J_l \tag{A1}$$

$$\text{Volume flow ratio } \xi = \frac{Q_g}{Q_g + Q_l} \tag{A2}$$

$$\text{Void fraction } \varepsilon = J_g/U_b \tag{A3}$$

$$\text{Capillary number } Ca = \mu_l \cdot U_b/\sigma_l \tag{A4}$$

$$\text{At the bubble cross section : } U_b \cdot A_b + U_f A_f = Q_l + Q_g \tag{A5}$$

Eq. (A5) represents mass continuity derived from the control volume approach and will hold for all cross-sections along the channel [58]. So, at the slug cross-section:

$$U_b A_b = 0;\quad U_f A_f = U_s A \Rightarrow U_s = \frac{Q_g + Q_l}{A} = J_{tot} \tag{A6}$$

$$(J_{tot} - U_b) \cdot A = (U_l(z) - U_b) \cdot A_l(z) \tag{A7}$$

where $U_l(z)$ and $A_l(z)$ are the mean cross-sectional velocity and the cross-section area of the liquid at a certain axial position $z$, respectively.

$$\text{Slip ratio } \psi = \frac{U_b}{U_s} = \frac{U_b}{J_{tot}} = \frac{\xi}{\varepsilon} \tag{A8}$$

$$m = \frac{U_b - U_s}{U_b} = 1 - \frac{1}{\psi} \tag{A9}$$

## References

[1] V.S. Ajaev, G.M. Homsy, Modeling shapes and dynamics of confined bubbles, Annual Review of Fluid Mechanics 38 (2006) 277–307.
[2] T. Cubaud, C.M. Ho, Transport of bubbles in square microchannels, Physics of Fluids 16 (2004) 4575–4585.

[3] J.D. Chen, Measuring the film thickness surrounding the bubble inside a capillary, Journal of Colloid and Interface Science 109 (1986) 341–349.
[4] K.A. Triplett, S.M. Ghiaasiaan, A. Khalik, S.I. Le-Mouel, B.N. McCord, Gas–liquid two-phase flow in microchannels. Part I: two-phase flow pattern, International Journal of Multiphase Flow 25 (1999) 377–394.
[5] S.M. Ghiaasiaan, S.I. Abdel-Khalik, Two-phase flow in microchannels, Advances in Heat Transfer 34 (2001) 145–254.
[6] S. Devesenathipathy, J.G. Santiago, S.T. Werely, C.D. Meinhart, K. Takhera, Particle imaging techniques for micro-fabricated fluidic systems, Experiments in Fluids 34 (2003) 504–514.
[7] D. Spernjak, A.K. Prasad, S.G. Advani, Experimental investigation of liquid water formation and transport in a transparent single-serpentine PEM fuel cell, Journal of Power Sources 170 (2007) 334–344.
[8] V. van Steijn, M.T. Kreutzer, C.R. Kleijn, Velocity fluctuations of segmented flow in microchannels, Chemical Engineering Journal 135 (2008) 159–165.
[9] M.K. Moharana, N.R. Peela, S. Khandekar, D. Kunzru, Distributed hydrogen production from ethanol in a microfuel processor: issues and challenges, Renewable and Sustainable Energy Reviews 15 (2011) 524–533.
[10] J. Fabre, A. Liñe, Modeling of two-phase slug flow, Annual Review of Fluid Mechanics 24 (1992) 21–46.
[11] T.C. Thulasidas, M.A. Abraham, R.L. Cerro, Bubble train flow in capillaries of circular and square cross section, Chemical Engineering Science 50 (1995) 183–199.
[12] T.C. Thulasidas, M.A. Abraham, R.L. Cerro, Flow patterns in liquid slugs during bubble train flow inside capillaries, Chemical Engineering Science 52 (17) (1997) 2947–2962.
[13] K. Moriyama, A. Inoue, Thickness of the liquid film formed by a growing bubble in a narrow gap between two horizontal plates, Transactions of ASME Journal of Heat Transfer 118 (1996) 132–139.
[14] S. Nogueira, R.G. Sousa, A.M.F.R. Pinto, M.L. Riethmuller, J.B.L.M. Campos, Simultaneous PIV and shadowgraphy in slug flow: a solution for optical problems, Journal of Experimental Fluids 35 (2003) 598–609.
[15] S. Nogueira, M.L. Riethmuller, J.B.L.M. Campos, A.M.F.R. Pinto, Flow patterns in the wake of a Taylor bubble rising through vertical columns of stagnant and flowing Newtonian liquids: an experimental study, Chemical Engineering Science 61 (22) (2006) 7199–7212.
[16] P. Angeli, A. Gavriilidis, Hydrodynamics of Taylor flow in small channels: a review, Proceedings of IMechE, Part C: Journal of Mechanical Engineering Science 222 (2008) 737–751.
[17] V. van Steijn, M.T. Kreutzer, C.R. Kleijn, μ-PIV study of the formation of segmented flow in microfluidic T-junctions, Chemical Engineering Science 62 (24) (2007) 7505–7514.
[18] C. King, E. Walsh, R. Grimes, PIV measurements of flow within plugs in a microchannel, Microfluids and Nanofluids 3 (2007) 463–472.
[19] G. Berčič, A. Pintar, The role of gas bubbles and liquid slug lengths on mass transport in the Taylor flow through capillaries, Chemical Engineering Science 52 (1997) 3709–3719.
[20] B. Mehta, S. Khandekar, Infra-red thermography of laminar heat transfer during early thermal development inside a square mini-channel, Experimental Thermal and Fluid Science 42 (2012) 219–229.
[21] F.P. Bretherton, The motion of long bubbles in tubes, Journal of Fluid Mechanics 10 (1961) 166–188.
[22] T.Z. Harmathy, Velocity of large drops and bubbles in media of infinite or restricted extent, AIChE Journal 6 (2) (1960) 281–288.
[23] E.T. White, R.H. Beardmore, The velocity of rise of single cylindrical air bubbles through liquids contained in vertical tubes, Chemical Engineering Science 17 (1962) 351–361.
[24] F. Fairbrother, A.E. Stubbs, The bubble tube method of measurement, Journal of the Chemical Society 1 (1935) 527–529.
[25] G.I. Taylor, Deposition of a viscous fluid on the wall of a tube, Journal of Fluid Mechanics 10 (1961) 161–163.
[26] B.G. Cox, An experimental investigation of streamlines in viscous fluid expelled from a tube, Journal of Fluid Mechanics 20 (1964) 193–200.
[27] M.D. Giavedoni, F.A. Saita, The axisymmetric and plane case of a gas phase steadily displacing a Newtonian liquid – a simultaneous solution to the governing equations, Physics of Fluids 9 (8) (1997) 2420–2428.
[28] T. Taha, Z.F. Cui, Hydrodynamics of slug flow inside capillaries, Journal of Chemical Engineering Science 59 (2004) 1181–1190.
[29] T. Taha, Z.F. Cui, CFD modeling of slug flow inside square capillaries, Chemical Engineering Science 61 (2006) 665–675.
[30] M.N. Kashid, I. Gerlach, S. Goetz, J. Franzke, J.F. Acker, F. Platte, D.W. Agar, S. Turek, Internal circulation within the liquid slugs of a liquid–liquid slug-flow capillary microreactor, Industrial and Engineering Chemistry Research 44 (2005) 5003–5010.
[31] W.B. Kolb, R.L. Cerro, The motion of long bubbles in tubes of square cross sections, Physics of Fluids A 5 (1993) 1549–1557.
[32] F. Kamisli, Flow of a long bubble in a square capillary, Chemical Engineering and Processing 42 (2003) 351–363.
[33] L.W. Schwartz, H.M. Princen, A.D. Kiss, On the motion of bubbles in capillary tubes, Journal of Fluid Mechanics 172 (1986) 259–275.
[34] J. Ratulowski, H.C. Chang, Transport of gas bubbles in capillaries, Physics of Fluids A 1 (10) (1989) 1642–1655.
[35] J.M. Van Baten, R. Krishna, CFD simulations of mass transfer from Taylor bubbles rising in circular capillaries, Chemical Engineering Science 59 (2004) 2535–2545.
[36] J.M. Van Baten, R. Krishna, CFD simulations of wall mass transfer for Taylor flow in circular capillaries, Chemical Engineering Science 60 (2005) 1117–1126.
[37] H. Ide, H. Matsumura, Frictional pressure drops of two phase gas liquid flow in rectangular channels, Experimental Thermal and Fluid Science 3 (1990) 362–372.
[38] K. Mishima, T. Hibiki, H. Nishihera, Some characteristics of gas liquid flow in narrow rectangular ducts, International Journal of Multiphase Flow 19 (1993) 115–124.
[39] M.W. Wambsganss, J.K. Jendrzejczyk, D.M. France, N.T. Obot, Frictional pressure gradients in two phase flow in a small horizontal rectangular channel, Experimental Thermal and Fluid Science 5 (1992) 40–56.
[40] I.Y. Chen, Y.M. Chen, B.C. Yang, C.C. Wang, Two phase flow pattern and frictional performance across small rectangular channels, Applied Thermal Engineering 29 (2009) 1309–1318.
[41] Y. Han, N. Shikazono, Measurements of liquid film thickness in micro square channel, International Journal of Multiphase Flow 35 (2009) 896–903.
[42] M. Wörner, A key parameter to characterize Taylor flow in narrow circular and rectangular channels, in: 7th Int. Conf. Multiphase Flow (ICMF 2010), Tampa, FL, USA, May 30–June 4, 2010.
[43] Z.Y. Bao, D.F. Fletcher, B.S. Haynes, An experimental study of gas liquid flow in a narrow conduit, International Journal of Heat and Mass Transfer 43 (2000) 2313–2324.
[44] C. Narayanan, D. Lakehal, Two phase convective heat transfer in miniature pipes under normal and micro-gravity conditions, Journal of Heat Transfer 130 (2008) 074502.
[45] R. Gupta, D.F. Fletcher, B.S. Haynes, CFD modelling of flow and heat transfer in the Taylor flow regime, Chemical Engineering Science 65 (2010) 2094–2107.
[46] A.P. Walsh, J.E. Walsh, S.Y. Muzychka, Heat transfer model for gas–liquid slug flows under constant flux, International Journal of Heat and Mass Transfer 53 (2010) 3193–3201.
[47] A.N. Asadolahi, R. Gupta, D.F. Fletcher, B.S. Haynes, CFD approaches for the simulation of hydrodynamics and heat transfer in Taylor flow, Chemical Engineering Science 66 (2011) 5575–5584.
[48] A. Mehdizadeh, S.A. Sherif, W.E. Lear, Numerical simulation of thermofluid characteristics of two-phase slug flow in microchannels, International Journal of Heat and Mass Transfer 54 (2011) 3457–3465.
[49] A.N. Asadolahi, R. Gupta, S.S.Y. Leung, D.F. Fletcher, B.S. Haynes, Validation of a CFD model of Taylor flow hydrodynamics and heat transfer, Chemical Engineering Science 69 (2012) 541–552.
[50] S.S.Y. Leung, R. Gupta, D.F. Fletcher, B.S. Haynes, Gravitational effect on Taylor flow in horizontal microchannels, Chemical Engineering Science 69 (2012) 553–564.
[51] P. Zaloha, J. Kristal, V. Jiricny, N. Volkel, C. Xuereb, J. Aubin, Characteristics of liquid slugs in gas–liquid Taylor flow in microchannels, Chemical Engineering Science 68 (2012) 640–649.
[52] V. Talimi, Y.S. Muzychka, S. Kocabiyik, Numerical simulation of the pressure drop and heat transfer of two phase slug flows in microtubes using moving frame of reference technique, International Journal of Heat and Mass Transfer 55 (2012) 6463–6472.
[53] V. Talimi, Y.S. Muzychka, S. Kocabiyik, A review on numerical studies of slug flow hydrodynamics and heat transfer in microtubes and microchannels, International Journal of Multiphase Flow 39 (2012) 88–104.
[54] S. Hayashi, N. Kasagi, Y. Suzuki, The effects of inlet flow conditions on gas–liquid two-phase flow in a micro tube, in: Proc. HT2007 and 2007 ASME-JSME Thermal Engineering Summer Heat Transfer Conference, HT2007-32916, 2007.
[55] A.A. Armand, G.G. Treschev, The resistance during the movement of a two-phase systems in horizontal pipe, Izvestiya Vsesojuznogo Teplotekhnicheskogo Instituta 1 (1946) 16–23.
[56] R.K. Shah, L.A. London, Laminar Flow Forced Convection in Ducts, Academic Press Inc, 1978, ISBN 0120200511.
[57] S.S.Y. Leung, Y. Liu, D.F. Fletcher, B.S. Haynes, Heat transfer in well-characterised Taylor flow, Chemical Engineering Science 65 (2010) 6379–6388.
[58] M. Suo, P. Griffith, Two-phase flow in capillary tubes, Journal of Basic Engineering (1964) 86576–86582.